Global Journal of Researches in Engineering: J
General Engineering
Volume 18 Issue 1 Version 1.0 Year 2018
Type: Double Blind Peer Reviewed International Research Journal
Publisher: Global Journals
Online ISSN: 2249-4596 & Print ISSN: 0975-5861

Thermo Dynamic Analysis on MHD Casson Nano-Fluid Flow in a Vertical Porous Space with Stretching Walls

By R.K. Selvi, R. Muthuraj & S. Srinivas
VIT-AP University

Abstract- This work is concerned with MHD Casson nanofluid flow in a vertical porous space with heat and mass transfer in the presence of chemical reaction. The governing non-linear partial differential equations are reduced to ordinary differential equation by employing the similarity transformations then it solved by homotopy analysis method (HAM). The results are presented with the help of graphs for different values of the involved parameters and discussed. It is found that increasing Brownian motion parameter, thermophoresis parameter and Prandtl number are lead to promote fluid temperature significantly than other parameters. Also, it is observed that increasing Lewis number lead to enhance the concentration field whereas the opposite trend can be noticed with increasing thermal parameters. Further, we have compared HAM solution with the numerical solution by using ND solver in Mathematica.

Keywords: homotopy analysis method, MHD, chemical reaction, stretching walls.

GJRE-J Classification: FOR Code: 020304

THERMODYNAMICANALYSISONMHDCASSONNANOFLUIDFLOWINAVERTICALPOROUSSPACEWITHSTRETCHINGWALLS

Strictly as per the compliance and regulations of:

Thermo Dynamic Analysis on MHD Casson Nano-Fluid Flow in a Vertical Porous Space with Stretching Walls

R.K. Selvi [α], R. Muthuraj [σ] & S. Srinivas [ρ]

Abstract- This work is concerned with MHD Casson nanofluid flow in a vertical porous space with heat and mass transfer in the presence of chemical reaction. The governing non-linear partial differential equations are reduced to ordinary differential equation by employing the similarity transformations then it solved by homotopy analysis method (HAM). The results are presented with the help of graphs for different values of the involved parameters and discussed. It is found that increasing Brownian motion parameter, thermophoresis parameter and Prandtl number are lead to promote fluid temperature significantly than other parameters. Also, it is observed that increasing Lewis number lead to enhance the concentration field whereas the opposite trend can be noticed with increasing thermal parameters. Further, we have compared HAM solution with the numerical solution by using ND solver in Mathematica.

Keywords: homotopy analysis method, MHD, chemical reaction, stretching walls.

I. Introduction

The problem of mixed convective flow in vertical channels with different wall temperatures has a number of important engineering applications such as microelectronic components cooling, in the design of compact heat exchangers, industrial furnaces, power engineering and so on. Also, convection flows with heat and mass transfer under the influence of a magnetic field, chemical reaction occurs in many branches of engineering applications and transport processes in industrial applications such as chemical industry, power and cooling industry for drying, chemical vapour deposition on surfaces, cooling of nuclear reactors and MHD power generators (See Refs. [1-10]). Moreover, MHD channel flows gained significant theoretical and practical importance owing to their applications in MHD generators, accelerators and blood flow measurements. In view of these applications, Srinivas et al. [7] have studied the effects of thermal-diffusion and diffusion-thermo effects in a two-dimensional viscous flow between slowly expanding or contracting walls with weak permeability.

The effect of chemical reaction and thermal radiation on MHD flow over an inclined permeable stretching surface with non-uniform heat source was examined by Srinivas et al. [8]. Later, Muthuraj et al. [9] discussed the combined effects of thermal-diffusion and diffusion-thermo with space porosity on MHD mixed convective flow of micropolar fluid in a vertical channel. Immaculate et al. [10] have investigated the influence of thermophoretic particle deposition on fully developed MHD mixed convective flow in a vertical channel with thermal-diffusion and diffusion-thermo effects. More recently, effects of thermal diffusion and diffusion thermo on MHD Couette flow of Powell-Eyring fluid in an inclined porous space in the presence of chemical reaction was investigated by Muthuraj et al. [11].

In engineering applications, the flows of non-Newtonian fluid have been attracting researchers significantly during the past few decades. In particular, it occurs in the extrusion of polymer fluids, cooling of metallic plate in the bath, exotic lubricants, artificial gels, natural gels, colloidal and suspension solutions. The most important among these fluids is the Casson fluid. It can be defined as a shear thinning liquid which is assumed to have an infinite viscosity at zero rate of shear, a yield stress below which no flow occurs and a zero viscosity at an infinite rate of shear. Human blood can also be treated as a Casson fluid due to the blood cells' chain structure and the substances contained like protein, fibrinogen, rouleaux etc [16]. Hence the Casson fluid has its own importance in scientific as well as in engineering areas. Many researchers have used the Casson fluid model for mathematical modeling of blood flow in narrow arteries at low shear rates (See Refs.[12-18]). Nadeem et al. [15] examined MHD flow of a Casson fluid over an exponentially shrinking sheet. Sarojamma et al.[16] have investigated MHD Casson fluid flow with heat and mass transfer in a vertical channel with stretching walls. Arthur et al.[17] have analyzed of Casson fluid flow over a vertical porous surface with chemical reaction in the presence of magnetic field. More recently, the unsteady MHD free flow of a Casson fluid past an oscillating vertical plate with constant wall temperature was analyzed by Khalid et al.[18].

Author α σ: Department of Mathematics, PSNA College of Engineering & Technology, Dindigul-624622, India.
Author ρ: Department of Mathematics, VIT – AP University, Inavolu Amaravati, Andhra Pradesh-522 237, India.
e-mail: dr.ramamoorthymuthuraj@gmail.com

Global Journal of Researches in Engineering (J) Volume XVIII Issue I Version I Year 2018

Nanoparticle research is currently an area of intense scientific interest due to a wide variety of potential applications in biomedical, optical and electronic fields. It is a microscopic particle with at least one dimension less than 100 nm. Many existing studies indicate that an enormous enhancement in the emission intensity, quantum yield, and lifetime of the molecular rectangles has been observed when the solvent medium is changed from organic to aqueous and it clearly exhibit enhanced thermal conductivity, which goes up with increasing volumetric fraction of nanoparticles[19-28]. The model of nanofluid was first developed by Choi [19]. Later, fully developed mixed convection flow between two paralleled vertical flat plates filled by a nanofluid with the Buongiorno mathematical model using HAM was analyzed by Xu et al. [25]. Nadeem et al. [26] presented the steady stagnation point flow of a Casson nanofluid in the presence of convective boundary conditions. Khan et al. [27] analyzed the fully-developed two-layer Eyring–Powell fluid in a vertical channel divided into two equal regions. One region is filled with the clear Eyring–Powell fluid and the other with the Eyring–Powell nanofluid. The problem of MHD laminar free convection flow of nanofluid past a vertical surface was analyzed by Freidoonimehr [28]. More recently, Immaculate et al. [29] examined the MHD unsteady flow of Williamson nanofluid in a vertical channel filled with a porous material and oscillating wall temperature using HAM. To the best of our knowledge MHD Casson nanofluid in a vertical channel with stretching walls has not been studied before. In this paper, we therefore propose to analyzed the steady fully-developed mixed convection flow of MHD Casson nanofluid in a vertical porous space with stretching walls in the presence of chemical reaction. It is important to note that this type of analysis has direct applications to the study of blood flow in the cardiovascular system subject to external magnetic field. The reduced non-dimensional, highly non-linear, coupled system of equations is solved by HAM [30-35]. The influence of significant parameters on heat and mass transfer characteristics of the flow is presented through graphs and discussed.

II. Formulation of The Problem

We consider MHD Casson nanofluid flow in a vertical porous space bounded by two stretching walls and are maintained at different temperatures, concentrations. The channel walls are at the positions y = -L and y = L, as shown in Fig.1. A constant magnetic field of strength B_0 is applied perpendicular to the channel walls. The fluids in the region of the parallel walls are incompressible, non-Newtonian and their transport properties are assumed to be constant.

The constitutive equation for the Casson fluid can be written as [16]

$$\tau_{ij} = \begin{cases} 2\left[\mu_B + \dfrac{\tau_y}{\sqrt{2\pi}}\right]e_{ij}\,,\ \pi > \pi_c \\ 2\left[\mu_B + \dfrac{\tau_y}{\sqrt{2\pi_c}}\right]e_{ij},\ \pi < \pi_c \end{cases} \tag{1}$$

where μ_B is the plastic dynamic viscosity of the non-Newtonian fluid, τ_y is the yield stress of the fluid, π is the product of the component of deformation rate with itself, namely, $\pi = e_{ij}e_{ij}$, and e_{ij} is the (i, j) th component of deformation rate, and π_c is critical value of this product based on non-Newtonian model. Under the above assumptions and usual Boussinesq approximation, the fluid flow is governed by the following equations (See Refs. [16, 25, 26])

$$\frac{\partial u}{\partial x} + \frac{\partial v}{\partial y} = 0 \tag{2}$$

$$\rho_f\left(u\frac{\partial u}{\partial x} + v\frac{\partial u}{\partial y}\right) = -\frac{\partial p}{\partial x} + \mu_f\left(1+\frac{1}{\beta}\right)\nabla^2 u - \sigma B_0^2 u - \frac{\mu_f \varphi^*}{k^*}u - \rho_f C_F u^2 + \rho_f g\beta_t(1-C_0)(T-T_0) + g\beta_c(\rho_p-\rho_f)(C-C_0) \tag{3}$$

$$\rho_f\left(u\frac{\partial v}{\partial x} + v\frac{\partial v}{\partial y}\right) = -\frac{\partial p}{\partial y} + \mu_f\left(1+\frac{1}{\beta}\right)\nabla^2 v - \frac{\mu_f \varphi^*}{k^*}v \tag{4}$$

$$u\frac{\partial T}{\partial x} + v\frac{\partial T}{\partial y} = \alpha^*\nabla^2 T + \tau^*\left[D_B\left(\frac{\partial C}{\partial x}\frac{\partial T}{\partial x} + \frac{\partial C}{\partial y}\frac{\partial T}{\partial y}\right) + \frac{D_T}{\overline{T}}\left\{\left(\frac{\partial T}{\partial x}\right)^2 + \left(\frac{\partial T}{\partial y}\right)^2\right\}\right] \tag{5}$$

$$u\frac{\partial C}{\partial x}+v\frac{\partial C}{\partial y}=D_B\nabla^2 C+\frac{D_T k_T}{\overline{T}}\nabla^2 T-k_1 C \tag{6}$$

The boundary conditions of the problem are

$$u=bx\ ,\ v=0,\ T=T_1\ ,\ C=C_1\ \text{ at }\ y=-L \tag{7}$$

$$u=bx\ ,\ v=0,\ T=T_2\ ,\ C=C_2\ \text{ at }\ y=L \tag{8}$$

where u and v are the velocity components in x and y directions, T_1 and T_2 are the wall temperatures $(T_2>T_1)$, C_1 and C_2 are the wall concentrations, $\overline{T}$ is the mean value of T_1 and T_2, C_F is the inertial coefficient, C_p is the specific heat, B_0 is the transverse magnetic field, D_B is the Brownian diffusion coefficient, D_T is the thermophoresis diffusion coefficient, *g* is the acceleration due to gravity, p is the pressure, T is the temperature, k^* is the permeability of the medium, K is the thermal conductivity of the fluid, $\alpha^*=\frac{K}{(\rho C_p)_f}$ is the thermal diffusivity of the fluid, $\tau^*=\frac{(\rho C_p)_p}{(\rho C_p)_f}$, b>0 is the stretch of the channel walls, respectively, $\beta=\frac{\mu_B\sqrt{2\pi_c}}{\tau_y}$ is the Casson parameter, ρ_f,ρ_p densities of the base fluid and nanoparticle, respectively, $(\rho C_p)_f$ is the heat capacity of the fluid, $(\rho C_p)_p$ gives the effective heat capacity of the nanoparticle material, ν is the kinematic viscosity, φ^* is the porosity of the medium, μ_f is the dynamic viscosity of the fluid, σ is the coefficient of electric conductivity, β_t is the coefficient of thermal expansion, β_c is the coefficient of expansion with concentration and $\nabla^2=\frac{\partial^2}{\partial x^2}+\frac{\partial^2}{\partial y^2}$.

We introduce the similarity variables

$$u=bxf'(\eta)\ ;\ v=-Lbf(\eta)\ ;\ \eta=\frac{y}{L}\ ;\theta=\frac{T-T_1}{T_2-T_1}\ ;\ \ \phi=\frac{C-C_1}{C_2-C_1} \tag{9}$$

Invoking the above similarity variables to equations (3)-(6) and eliminating pressure gradient, we get

$$\left(1+\frac{1}{\beta}\right)f^{iv}-R_e\left(f'f''-ff'''\right)-Hf''-I\,f'f''+G_r\theta'+G_c\phi'=0 \tag{10}$$

$$\theta''+P_r[N_b\phi'\theta'+N_t(\theta')^2+R_e f\theta']=0 \tag{11}$$

$$\phi''+\frac{N_t}{N_b}\theta''+L_e(R_e f\phi'-\gamma\phi+k_1^*)=0 \tag{12}$$

The corresponding boundary conditions are:

$$f'=1\,,f=0\,,\theta=0\,,\phi=0\ \text{ at }\ \eta=-1 \tag{13}$$

$$f'=1\,,f=0\,,\theta=1,\ \phi=1\ \text{ at }\ \eta=1 \tag{14}$$

Where $H=M+\frac{1}{D_a}$, $k_1^*=\frac{-k_1C_1L^2}{\nu_f(C_2-C_1)}$ $I=\frac{2C_F bxL^2}{\nu_f}$ is the inertia coefficient, $R_e=\frac{L^2 b}{\nu_f}$ is the Reynolds number, $M=\sqrt{\frac{\sigma B_0^2L^2}{\mu_f}}$ is the Hartmann number,

$D_a = \frac{k^*}{\varphi^* L^2}$ is the permeability parameter, $G_r = \frac{g\beta_t(1-C_0)(T_2-T_1)L^2}{\nu_f bx}$ local temperature Grashof number , $G_c = \frac{g\beta_c(\rho_p-\rho_f)(C_2-C_1)L^2}{\mu_f bx}$ is the local nano-particle Grashof number, $P_r = \frac{\nu_f}{\alpha^*}$ is the Prandtl number, $L_e = \frac{\nu_f}{D_B}$ is the Lewis number, $N_b = \frac{\tau^* D_B(C_2-C_1)}{\nu_f}$ is the Brownian motion parameter $N_t = \frac{\tau^* D_T(T_2-T_1)}{\overline{T}\nu_f}$ is the thermophoresis parameter, $\gamma = \frac{k_1 L^2}{\nu_f}$ is the chemical reaction parameter.

The dimensionless volume flow rate $\overline{Q}$ is given by

$$\overline{Q} = \int_{-1}^{1} f' d\eta . \tag{15}$$

The skin friction coefficient, local heat rate transfer and the local mass diffusion rate at the walls are defined as

$$C_f = \frac{L\tau_w}{\mu_f bx} \; ; Nu = \frac{Lq_w}{K(T_2-T_1)} \; ; \; Sh = \frac{Lm_w}{D_B(C_2-C_1)}$$

$$\text{where } \tau_w = \mu_f\left(1+\frac{1}{\beta}\right)\left(\frac{\partial u}{\partial y}\right); \; q_w = -K\left(\frac{\partial T}{\partial y}\right); \; m_w = -D_B\left(\frac{\partial C}{\partial y}\right) \tag{16}$$

Its non-dimensional form is given by

$$C_f = \left(1+\frac{1}{\beta}\right) f''(\eta)\Big|_{\eta=\pm1} ; \; Nu = -\theta'(\eta)\Big|_{\eta=\pm1} ; \; Sh = -\phi'(\eta)\Big|_{\eta=\pm1} \tag{17}$$

III. Solution by Homotopy Analysis Method (HAM)

For HAM solutions, we can choose the initial guesses and auxiliary linear operators in the following form:

$$f_0(\eta) = \frac{\eta^3-\eta}{2}; \quad \theta_0(\eta) = \frac{1+\eta}{2}; \quad \phi_0(\eta) = \frac{1+\eta}{2} \tag{18}$$

$$L_1(f) = f^{iv} \quad L_2(\theta) = \theta'' \quad L_3(\phi) = \phi'' \tag{19}$$

with $L_1(c_1 + c_2\eta + c_3\eta^2 + c_4\eta^3) = 0$ $L_2(c_5\eta + c_6) = 0$ & $L_3(c_7\eta + c_8) = 0$, where $c_i (i = 1 \ldots 8)$ are constants and prime denotes the derivative with respect to η.

a) Zero-order deformation equations

Let $\wp \in [0,1]$ be an embedding parameter and h be the auxiliary non-zero parameter. We construct the following zero-order deformation equations.

$$(1-\wp)L_1[\hat{f}(\eta,\wp) - f_0(\eta)] = \wp h \mathbf{N}_1[\hat{f}(\eta,\wp), \hat{\theta}(\eta,\wp), \hat{\phi}(\eta,\wp)] \qquad \hat{f}(-1,\wp) = 0, \hat{f}(1,\wp) = 0 \tag{20}$$

$$(1-\wp)L_2[\hat{\theta}(\eta,\wp) - \theta_0(\eta)] = \wp h \mathbf{N}_2[\hat{f}(\eta,\wp), \hat{\theta}(\eta,\wp), \hat{\phi}(\eta,\wp)] , \qquad \hat{\theta}(-1,\wp) = 0, \hat{\theta}(1,\wp) = 1 \tag{21}$$

$$(1-\wp)L_3[\hat{\phi}(\eta,\wp) - \phi_0(\eta)] = \wp h \mathbf{N}_3[\hat{f}(\eta,\wp), \hat{\theta}(\eta,\wp), \hat{\phi}(\eta,\wp)] , \qquad \hat{\phi}(-1,\wp) = 0, \hat{\phi}(1,\wp) = 1 \tag{22}$$

where,

$$\mathbf{N}_1[\hat{f}(\eta,\wp), \hat{\theta}(\eta,\wp), \hat{\phi}(\eta,\wp)] =$$

$$\left(1+\frac{1}{\beta}\right)\hat{f}^{iv}(\eta,\wp) - R_e\left(\hat{f}'(\eta,\wp)\hat{f}''(\eta,\wp) - \hat{f}(\eta,\wp)\hat{f}'''(\eta,\wp)\right) - H\hat{f}''(\eta,\wp)$$

$$-I\,\hat{f}'(\eta,\wp)\hat{f}''(\eta,\wp) + G_r\hat{\theta}'(\eta,\wp) + G_c\hat{\phi}'(\eta,\wp)$$

Global Journal of Researches in Engineering (J) Volume XVIII Issue I Version I Year 2018

$$\mathbf{N}_2[\hat{f}(\eta,\wp),\hat{\theta}(\eta,\wp),\hat{\phi}(\eta,\wp)]$$
$$= \hat{\theta}''(\eta,\wp)+P_r[N_b\hat{\phi}'(\eta,\wp)\hat{\theta}'(\eta,\wp)+N_t\left(\hat{\theta}'(\eta,\wp)\right)^2+R_e\hat{f}(\eta,\wp)\hat{\theta}'(\eta,\wp)]$$

$$\mathbf{N}_3[\hat{f}(\eta,\wp),\hat{\theta}(\eta,\wp),\hat{\phi}(\eta,\wp)]=\hat{\phi}''(\eta,\wp)+\frac{N_t}{N_b}\hat{\theta}''(\eta,\wp)+L_e(R_e\hat{f}(\eta,\wp)\hat{\phi}'(\eta,\wp)-\gamma\hat{\phi}(\eta,\wp)+k_1^*)$$

For $\wp=0$ and $\wp=1$, we have

$$\hat{f}(\eta,0)=f_0(\eta) \quad \hat{f}(\eta,1)=f(\eta) \tag{23}$$

$$\hat{\theta}(\eta,0)=\theta_0(\eta) \quad \hat{\theta}(\eta,1)=\theta(\eta) \tag{24}$$

$$\hat{\phi}(\eta,0)=\phi_0(\eta) \quad \hat{\phi}(\eta,1)=\phi(\eta) \tag{25}$$

when $\wp$ increases from 0 to 1, then $\hat{f}(\eta,\wp)$, $\hat{\theta}(\eta,\wp)$, $\hat{\phi}(\eta,\wp)$ vary from initial guess $f_0(\eta)$, $\theta_0(\eta)$, $\phi_0(\eta)$ to the approximate analytical solution $f(\eta)$, $\theta(\eta)$, $\phi(\eta)$. By Taylor's theorem the series $\hat{f}(\eta,\wp)$, $\hat{\theta}(\eta,\wp)$, $\hat{\phi}(\eta,\wp)$ can be expressed as a power series of $\wp$ as follows,

$$\hat{f}(\eta,\wp)=f_0(\eta)+\sum_{m=1}^{\infty}f_m(\eta)\wp^m, \quad f_m(\eta)=\frac{1}{m!}\left.\frac{\partial^m\hat{f}(\eta,\wp)}{\partial\wp^m}\right|_{\wp=0} \tag{26}$$

$$\hat{\theta}(\eta,\wp)=\theta_0(\eta)+\sum_{m=1}^{\infty}\theta_m(\eta)\wp^m, \quad \theta_m(\eta)=\frac{1}{m!}\left.\frac{\partial^m\hat{\theta}(\eta,\wp)}{\partial\wp^m}\right|_{\wp=0} \tag{27}$$

$$\hat{\phi}(\eta,\wp)=\phi_0(\eta)+\sum_{m=1}^{\infty}\phi_m(\eta)\wp^m, \quad \phi_m(\eta)=\frac{1}{m!}\left.\frac{\partial^m\hat{\phi}(\eta,\wp)}{\partial\wp^m}\right|_{\wp=0}. \tag{28}$$

In which 'h' is chosen in such a way that these series are convergent at $\wp=1$, therefore we have

$$f(\eta)=f_0(\eta)+\sum_{m=1}^{\infty}f_m(\eta), \quad \theta(\eta)=\theta_0(\eta)+\sum_{m=1}^{\infty}\theta_m(\eta), \ \phi(\eta)=\phi_0(\eta)+\sum_{m=1}^{\infty}\phi_m(\eta) \tag{29}$$

b) The m-th order deformation equations

Differentiating the zero-order deformation Eqns. (20) - (22) m-times with respect to $\wp$ and then dividing them by $m!$ and finally setting $\wp=0$, we obtain the following m-th order deformation equations:

$$L_1[f_m(\eta)-\chi_m f_{m-1}(\eta)]=hR_m^f(\eta) \tag{30}$$

$$L_2[\theta_m(\eta)-\chi_m\theta_{m-1}(\eta)]=hR_m^\theta(\eta) \tag{31}$$

$$L_3[\phi_m(\eta)-\chi_m\phi_{m-1}(\eta)]=hR_m^\phi(\eta) \tag{32}$$

together with condition

$$f_m(-1)=0 \quad f_m(1)=0 \tag{33}$$

$$\theta_m(-1)=0 \quad \theta_m(1)=0 \tag{34}$$

$$\phi_m(-1)=0 \quad \phi_m(1)=0 \tag{35}$$

where,

$$R_m^f(\eta)=\left(1+\frac{1}{\beta}\right)f_{m-1}^{iv}-R_e\sum_{k=0}^{m-1}\left(f'_{m-k-1}f''_k-f_{m-k-1}f'''_k\right)-Hf''_{m-1}-I\sum_{k=0}^{m-1}f'_{m-k-1}f''_k+G_r\theta'_{m-1}+G_c\phi'_{m-1}$$

$$R_m^\theta(\eta)=\theta''_{m-1}+P_r\left(\sum_{k=0}^{m-1}\left[N_b\phi'_{m-k-1}\theta'_k+N_t\theta'_{m-k-1}\phi'_k+R_e f_{m-k-1}\theta'_k\right]\right)$$

Global Journal of Researches in Engineering (J) Volume XVIII Issue I Version I 5 Year 2018

$$R_m^{\phi}(\eta)=\phi_{m-1}^{''}+\frac{N_t}{N_b}\theta_{m-1}^{''}+L_e\left(R_e\sum_{k=0}^{m-1}f_{m-k-1}\phi_k^{'}-\gamma\phi_{m-1}+k_1^{*}(1-\chi_m)\right)$$

where,

$$\chi_m=\begin{cases}0 & \text{for} \quad m=1\\ 1 & \text{for} \quad m\neq 1\end{cases}.$$

IV. Convergence and the Residual Error

The convergence and rate of approximation for the HAM solution depends on auxiliary parameter 'h' (See Refs. [29-34]), for this purpose, we have plotted h-curves in Fig.2 with fixing the values of involved parameters G_r = 5, G_c = 5, R_e=1, I = 1, N_t = 0.45, N_b = 0.45, L_e = 10, M = 2, P_r = 2.5, $D_a=0.5$, $K_1=1$, $\gamma=0.5$, $\beta=0.6$. As a result, we can choose proper value of 'h' and also we obtain the optimal values of the auxiliary parameter 'h' by minimizing the average square residual error for the equations (10) to (12). We define the residual error for above mentioned equations as:

$$E_1=\left(1+\frac{1}{\beta}\right)f^{iv}-R_e\left(f^{'}f^{''}-ff^{'''}\right)-Hf^{''}-I\,f^{'}f^{''}+G_r\theta^{'}+G_c\phi^{'} \quad (36)$$

$$E_2=\theta^{''}+P_r[N_b\phi^{'}\theta^{'}+N_t(\theta^{'})^2+R_e f\theta^{'}] \quad (37)$$

$$E_3=\phi^{''}+\frac{N_t}{N_b}\theta^{''}+L_e(R_e f\phi^{'}-\gamma\phi+k_1^{*}) \quad (38)$$

where E_1, E_2 and E_3 are the residual error at m-th order of HAM approximation for f, θ and ϕ respectively. The average square residual error is given by:

$$\Delta_m=\frac{1}{3}\sum_{i=1}^{3}\int_{\eta=-1}^{\eta=1}E_i^2\,d\eta. \quad (39)$$

Further, we have tabulated the minimum average square residual errors for 10th, 15th, 20th, 25th order of HAM approximation for different values of parameters with optimal 'h' in Table 1. It is noted that the number of HAM approximation increases the corresponding minimum square residual error decreases significantly and hence it leads to more accurate solutions. Further, it is important to note that our present HAM solution is good agreement with Numerical solution which is obtained by NDSolve scheme of Mathematica (See Fig.9).

Table 1: The average square residual error for the optimal value of 'h' for different order of approxi-mations

Optimal h		Δ_m			
		10th order	15th order	20th order	25th order
-0.50	M = 5	4.48300x10^{-1}	2.17722 x10^{-2}	8.560151 x10^{-3}	6.293116 x10^{-3}
-0.46	β = 0.4	9.61660x10^{-1}	4.76619 x10^{-2}	1.085990 x10^{-2}	7.63834 0x10^{-3}
-0.28	γ = 1.5	2.41549 x10^{-1}	6.41384 x10^{-2}	1.741480 x10^{-2}	7.771010 x10^{-3}
-0.46	P_r = 1	3.23985x10^{-3}	8.82479 x10^{-4}	1.155850 x10^{-6}	1.230240 x10^{-8}
-0.51	N_t = 0.5	5.53236x10^{-1}	2.67400 x10^{-2}	1.01741 0x10^{-2}	6.737690 x10^{-3}
-0.49	N_b = 0.2	7.79008 x10^{-3}	7.15877 x10^{-3}	6.053300 x10^{-3}	6.032410 x10^{-3}
-0.58	L_e = 5	1.341560x10^{-1}	1.15096 x10^{-2}	7.017850 x10^{-3}	6.73713 0x10^{-3}

V. Results and Discussions

To study the behavior of solutions, numerical calculations for different values of magnetic parameter (M), Permeability parameter (D_a), Casson fluid parameter (β), thermophoresis parameter (N_t), Brownian motion parameter (N_b), Lewis number (L_e), Chemical reaction parameter (γ) and Prandtl number (P_r) have been carried out. Throughout the computations we employ G_r = 5, G_c = 5, $R_e=1$, I = 1, N_t = 0.45, N_b = 0.45, L_e = 10, M = 2, P_r = 2.5,

$D_a = 0.5$, $K_1 = 1$, $\gamma = 0.5$, $\beta = 0.6$ unless otherwise stated. Fig. 3a is prepared to see the influence of the Casson fluid parameter with two different values of magnetic parameter 'M' with fixed values of all other parameters. It is observe that magnitude of velocity is a decreasing function with increasing Casson fluid parameter and also we noted that increasing 'M' is lead to decelerate the velocity. Physically it means that the application of transverse magnetic field produces a resistive type force (Lorentz force) similar to drag force which tends to resist the fluid flow and thus reducing its velocity (as noted in [18]). The effect of permeability parameter D_a on the velocity is displayed in Fig. 3b. It depicts that the effect of increasing the value of D_a is to increase the velocity, which means that the drag force is reduced by increasing the value of the permeability parameter. Fig. 3c illustrates the influence of thermophoresis parameter N_t on velocity. It shows that increasing N_t is not shown much influence on velocity distribution. The quite similar effect can be noticed by varying Brownian motion parameter N_b on the velocity (See Fig.3d).

Fig. 4a is graphed to see the effect of Lewis number on temperature distribution. It is seen that temperature field is an increasing function in the left half of the channel whereas the behavior is reversed in the other region. Fig. 4b describes that, increasing chemical reaction parameter gives opposite behavior that of Fig.4a. Fig. 4c is plotted to see the influence of Brownian motion parameter on temperature distribution. It is evident that increasing N_b is to increase the fluid temperature significantly. The similar effect can be noticed with increasing N_t and P_r, which are shown in Figs.4d and 4e. Physically speaking, increasing thermal parameters is to increase momentum diffusivity, which leads to enhance the fluid temperature. Further, it is noted that N_t, P_r shows the significant influence on temperature field than other parameters. Fig. 5a shows the variation in concentration field with different values of Lewis number L_e. It depicts that increasing L_e lead to enhance species concentration significantly. Also, it is observed that when increasing L_e from 0 to 5 there is nearly 45% increase in concentration whereas increasing L_e from 5 to 10 there is only 20% (approx) decrease in the same, which means that low values of L_e dominates on concentration field. The opposite trend can be seen if L_e is replaced by chemical reaction parameter. (See Fig. 5b). Fig. 5c is prepared to see the effect of N_b on concentration. It is observed that concentration enhances with an increase of N_b whereas increasing thermal parameters N_t and P_r leads to suppress the concentration gradually (See Figs. 5d and 5e).

The variation of pressure gradient $\frac{dp}{dx}$ with M and G_r is plotted in Fig.6a. It is observed that increasing both the parameters lead to enhance the pressure gradient whereas in the absence of magnetic field pressure gradient is negative with increasing G_r, it means that high pressure gradient is need to promote the flow in the presence of magnetic field. The influence of inertia coefficient and material parameter on $\frac{dp}{dx}$ is graphed in Fig. 6b. It illustrates that pressure gradient is decreasing function with increasing I and β whereas very high pressure gradient exist for lower value of material parameter ($\beta < 0.5$). It indicates that more driving force is required for non-Newtonian fluid than Newtonian fluid. The variations on wall heat transfer rate (Nu) and wall mass transfer rate (Sh) with different values of N_b, N_t, L_e and γ are presented in Figs. 7 and 8 respectively. Influence of N_b and N_t on 'Nu' at both the walls is displayed in Fig 7. At the wall η=-1, 'Nu' is a decreasing function with increasing N_b, N_t whereas at the other wall there is no much influence with increasing N_b. Also, a sharp increment occurs in 'Nu' with increasing N_t. Variation on 'Sh' with different values of L_e and γ at both the walls is displayed in Fig 8. It depicts that, 'Sh' is a decreasing function with increasing L_e while increasing γ is not shown much influence at the wall η=-1. At the other wall, the opposite trend is noticed with increasing L_e.

VI. Conclusions

This article looks at flow, heat and mass transfer characteristics of a MHD Casson nanofluid in a vertical porous space with stretching walls in the presence of chemical reaction. HAM is adopted to obtain analytical solutions of the reduced set of ordinary differential equations. The results are presented through graphs for various values of the pertinent parameters and the salient features of the solutions are discussed graphically. This type of investigations is very important for mathematical modeling of blood flow in narrow arteries at low shear

Global Journal of Researches in Engineering (J) Volume XVIII Issue I Version I Year 2018

rates. It is found that magnitude of velocity is a decreasing function with the Casson fluid parameter and Hartmann number whereas increasing permeability parameter D_a. Increasing N_b, N_t and P_r are tends to promote the fluid temperature significantly. Concentration field significantly enhances with increasing L_e while increasing N_t and P_r suppresses the fluid concentration. Nusselt number distribution is a decreasing function with increasing N_b, N_t at the wall $\eta = -1$ while the parameter N_t tends to enhance at the other wall $\eta = 1$.

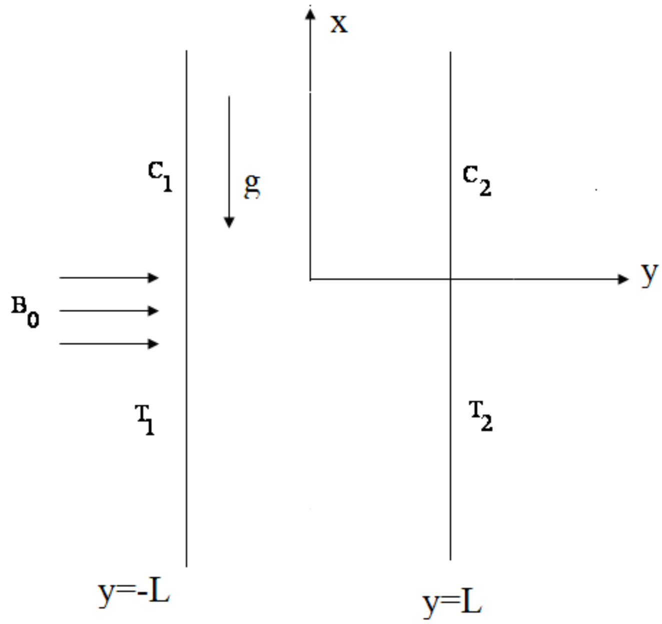

Fig. 1: Schematic diagram of the problem

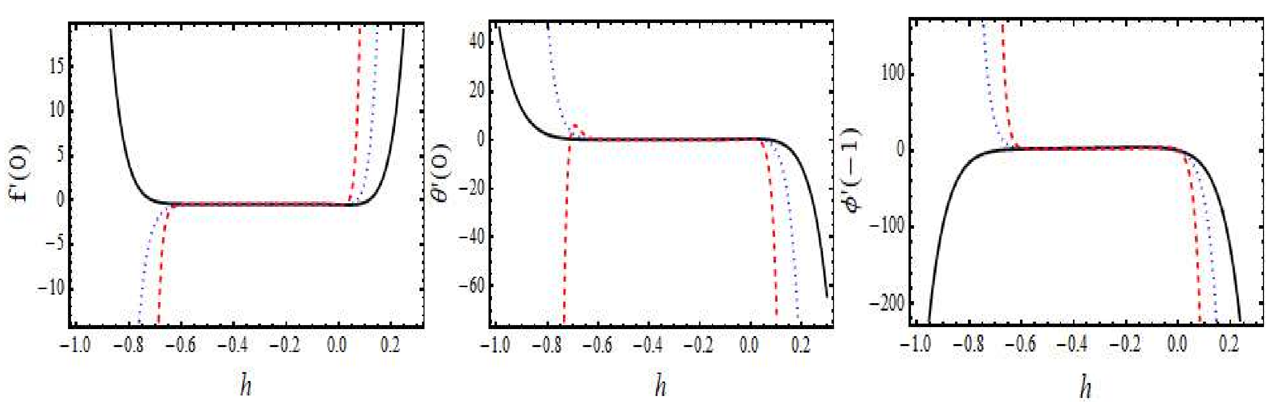

2: h-curves for velocity, temperature and concentration distribution
(___ 10^{th}, ... 15^{th}, - - - 25^{th} orders of approximation)

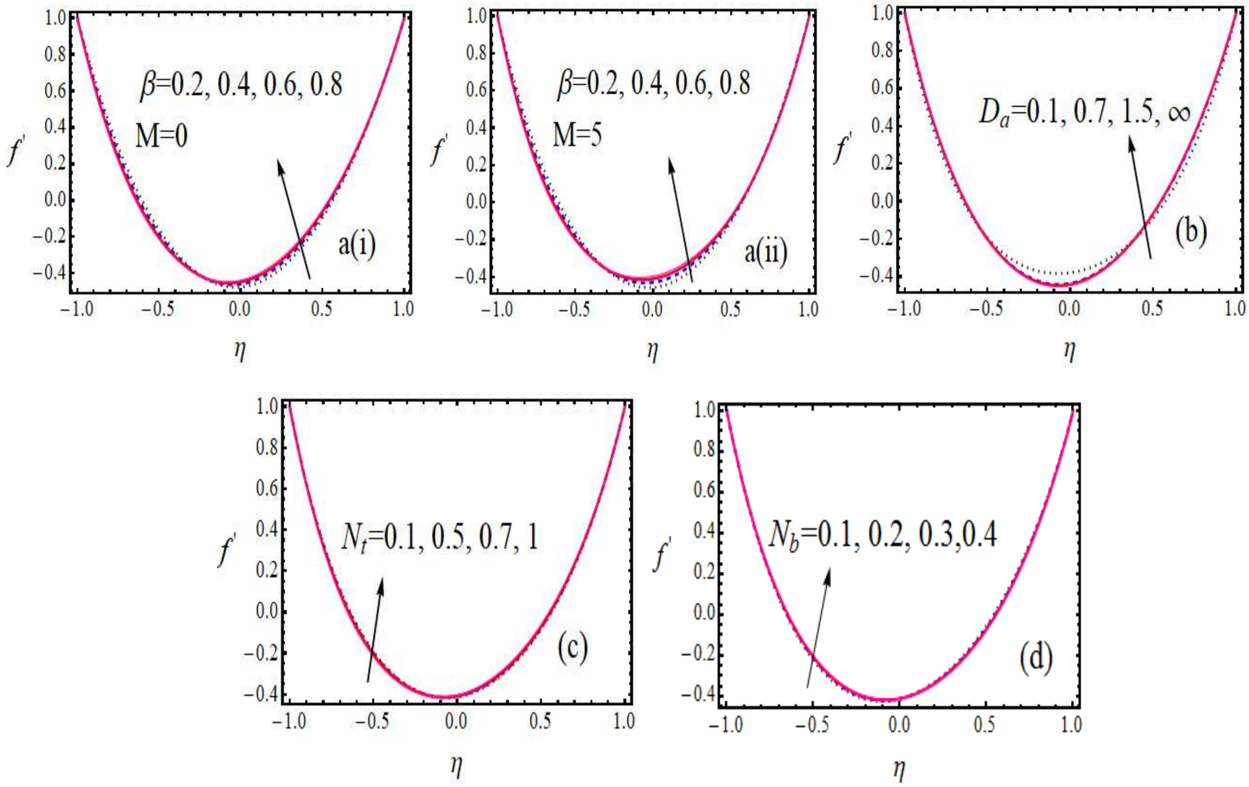

3: Effects of M, β, D_a, N_t and N_b on Velocity distribution

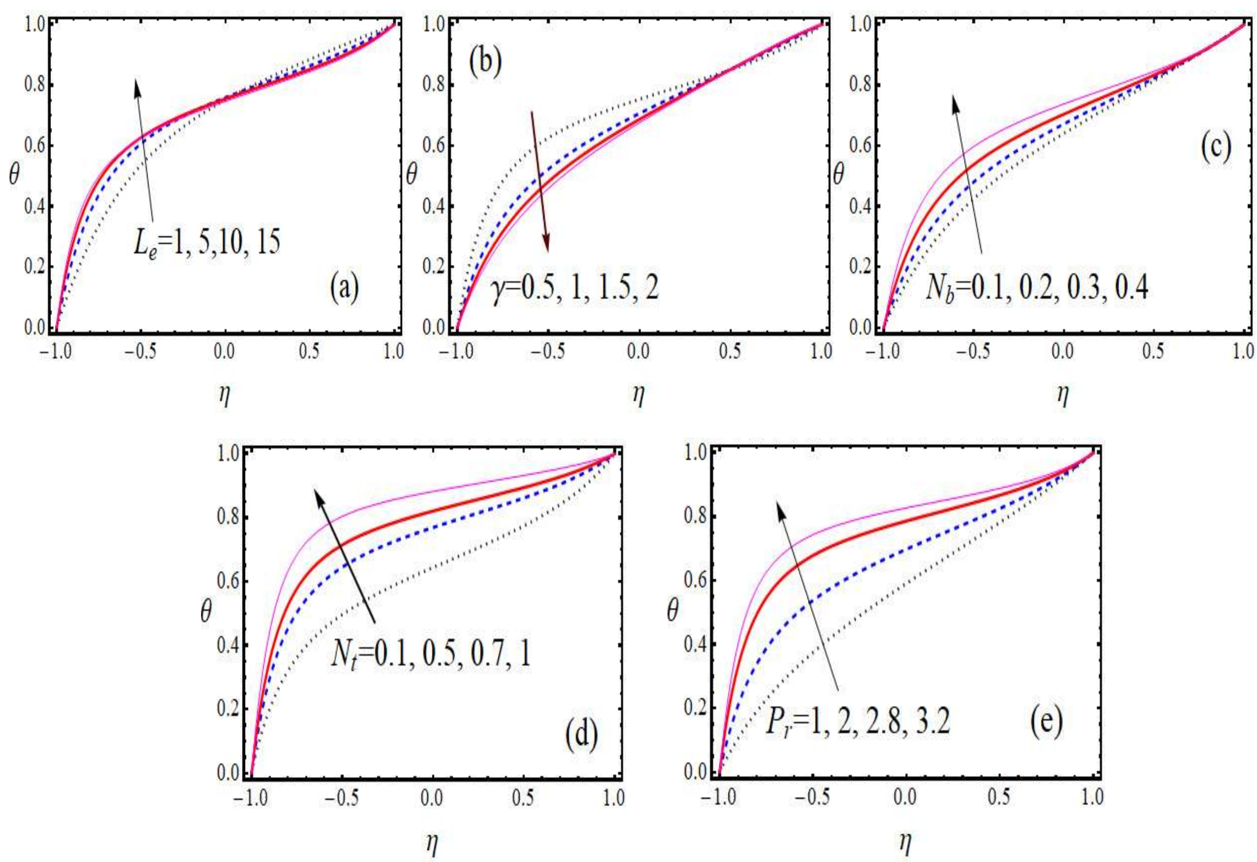

4: Effects of L_e, γ, N_b, N_t and P_r on Temperature distribution

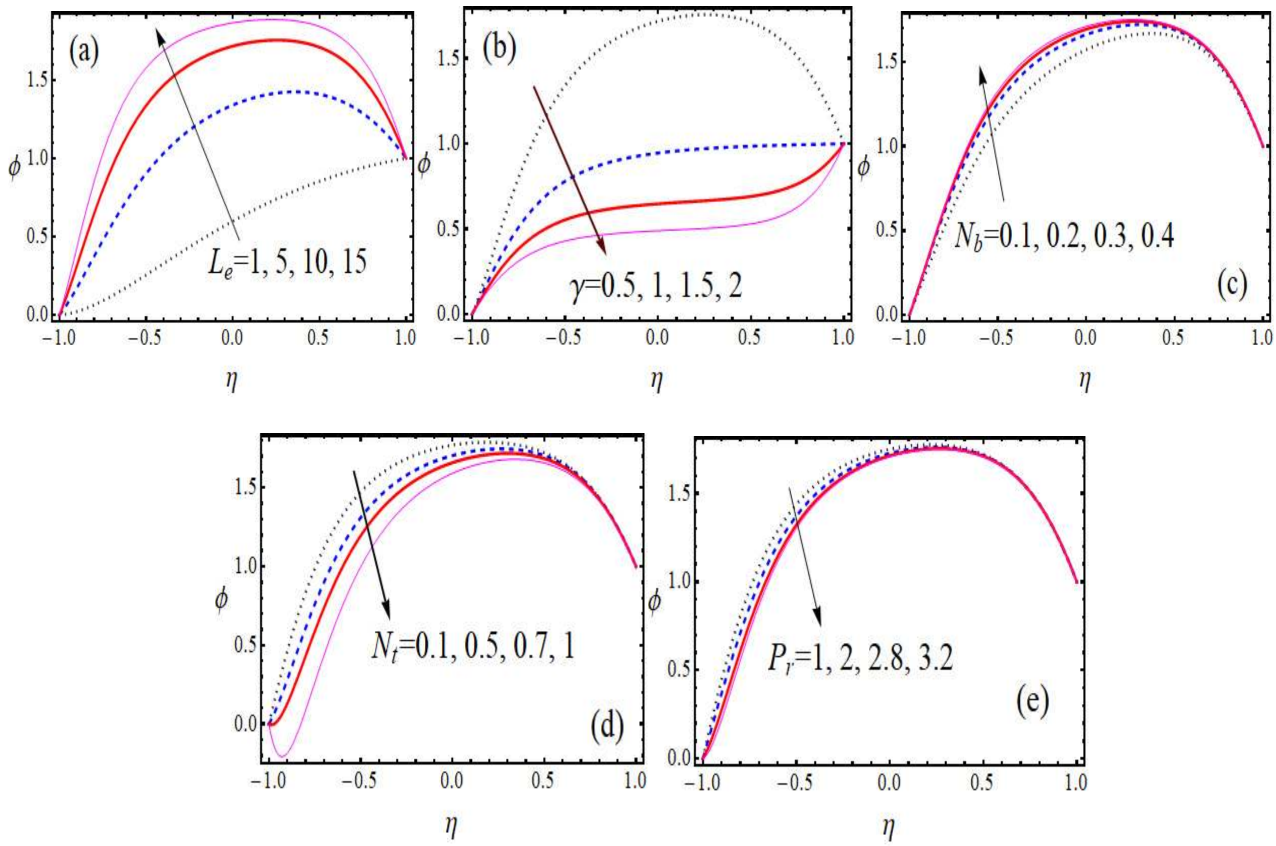

: Effects of L_e, γ, N_b, N_t and P_r on Concentration distribution

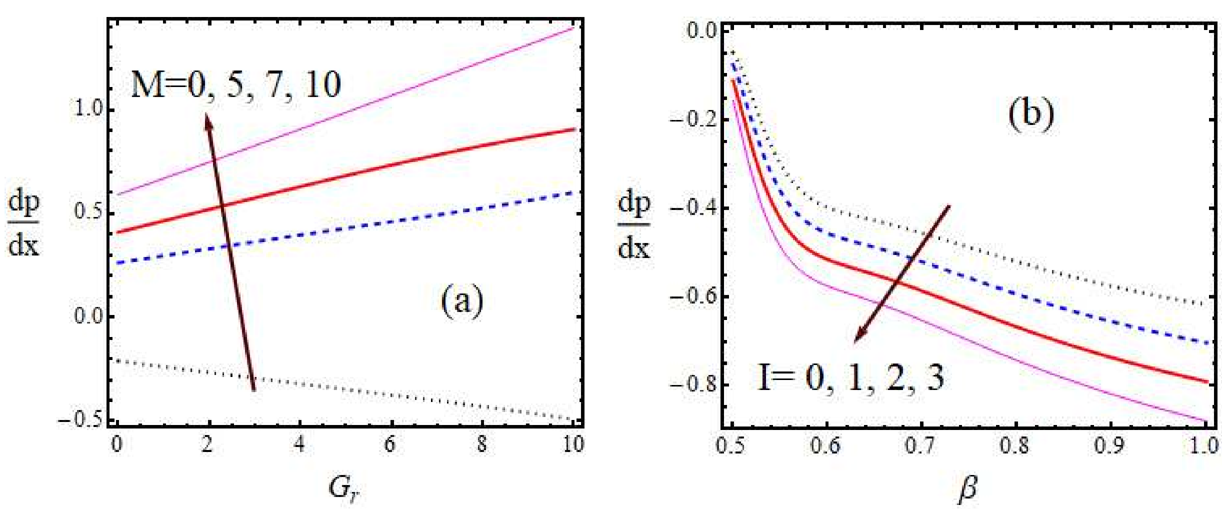

6: Effects of M and I on Pressure gradient distribution

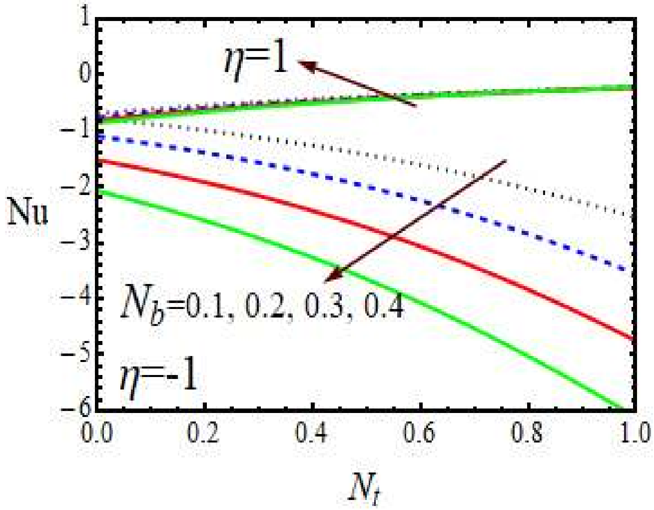

7: Effect of N_t on Nusselt number distribution

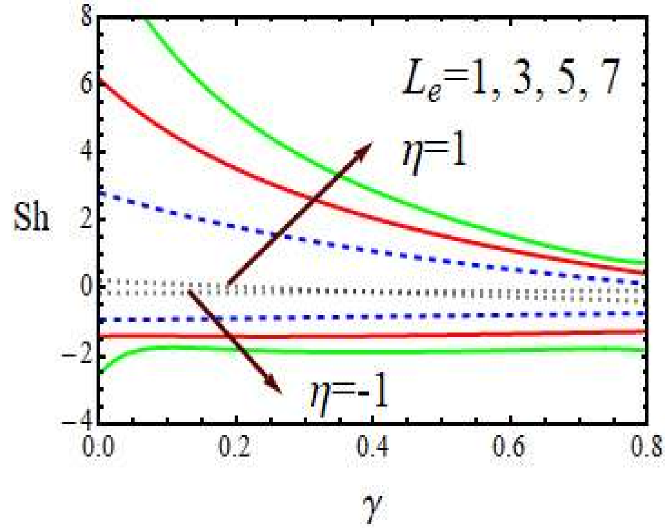

8: Effect of γ on Sherwood number distribution

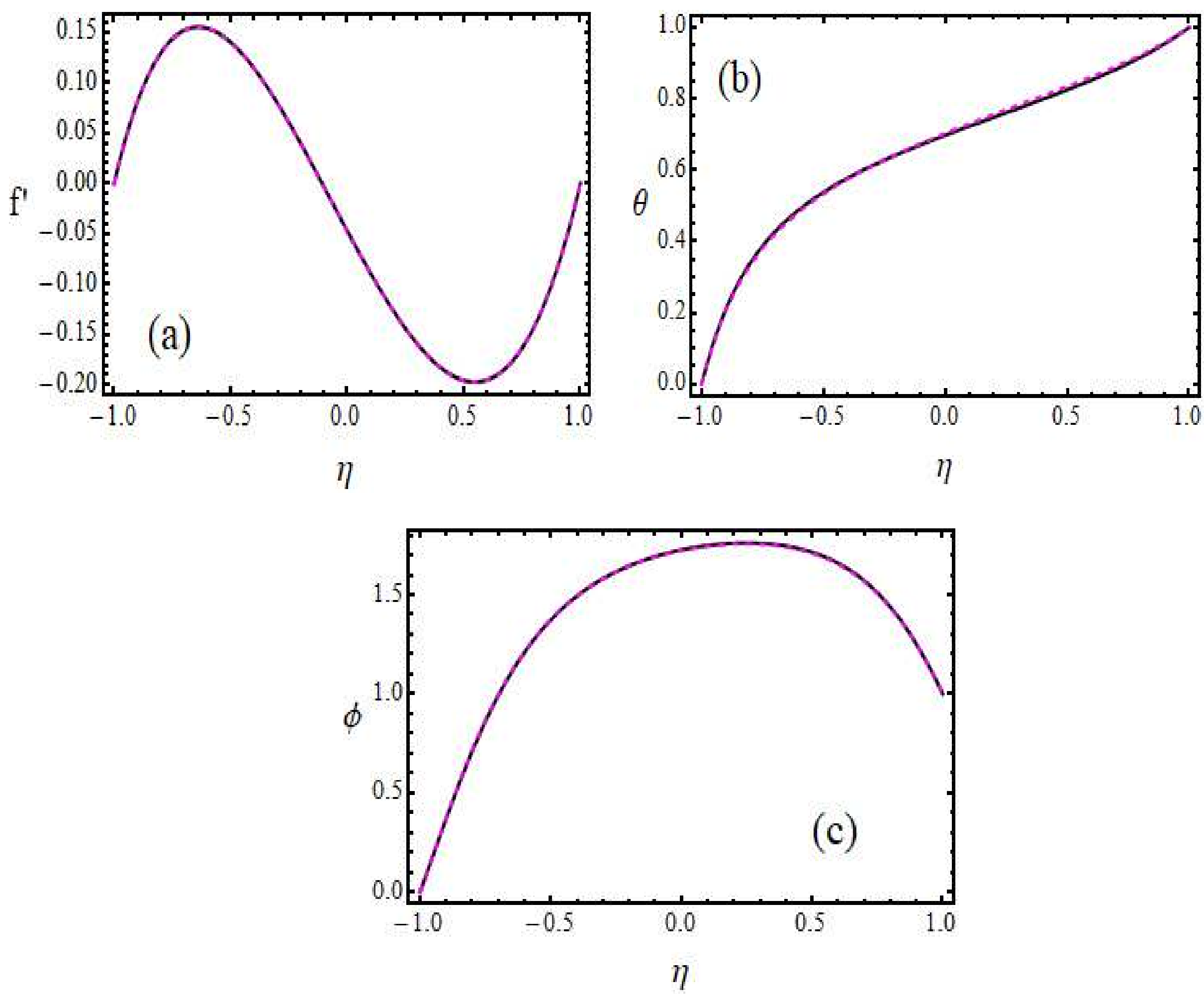

9: Comparison between ___HAM Solution and -----Numerical Solution

$(G_r = 5,\ G_c = 5,\ R_e = 1,\ l = 1,\ N_t = 0.45,\ N_b = 0.45,\ M = 2,$
$P_r = 2,\ D_a = 0.5,\ K_1 = 1,\ \gamma = 0.5,\ \beta = 0.6)$

NOMENCLATURE

B_0 Transverse magnetic field
$b>0$ Stretch of the channel walls(m)
C Dimensional concentration(Kg/m^3)
C_1, C_2 Wall concentrations (Kg/m^3)
C_0 Initial concentration (Kg/m^3)
C_F Inertial coefficient
C_p Specific heat
D_a Permeability parameter
D_B Brownian diffusion coefficient (m^2/s)
D_T Thermophoresis diffusion coefficient (m^2/s)
e_{ij} (i, j) th component of deformation rate
f Dimensionless stream function
f' Dimensionless velocity
g Acceleration due to gravity(m/sec^2)
G_r Local temperature Grashof number
G_c Local nano-particle Grashof number
I Inertia coefficient
k^* Permeability of the medium(m^2)
K Thermal conductivity of the fluid ($W/m\,K$)
L_e Lewis number
M Hartmann number
N_b Brownian motion parameter
N_t Thermophoresis parameter
p Pressure(N/m^2)
P_r Prandtl number
R_e Reynolds number
T Dimensional temperature
T_1, T_2 Wall temperatures (K)
$\bar{T}$ Mean value of T_1 and T_2 (K)
T_0 Inlet temperature (K)
u , v Dimensional velocity components in x and y directions (m/s)

Greek Symbols

α^* Thermal diffusivity of the fluid (m/s^2)
β Casson parameter
θ Dimensionless temperature
β_t Coefficient of thermal expansion(K^{-1})
β_c Coefficient of expansion with concentration(K^{-1})
μ_B Plastic dynamic viscosity of the non-Newtonian fluid ($N\,s/m^2$)
μ_f Dynamic viscosity of the fluid ($N\,sec/m^2$)
γ Chemical reaction parameter
ν Kinematic viscosity(m^2/sec)
ρ_f, ρ_p Densities of the base fluid and nano-particle (Kg/m^3)
$(\rho C_p)_f$ Heat capacity of the fluid(J/K)
$(\rho C_p)_p$ Effective heat capacity of the nanoparticle Material (J/K)
φ^* Porosity of the medium
ϕ Dimensionless fluid concentration
σ Coefficient of electric conductivity(S/m)
τ_y Yield stress of the fluid (N/m^2)
π Product of the component of deformation rate

Références

1. Riley N, Magneto-hydrodynamic free convection, J Fluid Mech., 18 (1964) 577- 586.
2. Raptis A, Massias C and Tzivanidis G, Hydromagnetic free convection flow through a porous medium between two parallel plates, Phys. Lett., 90A (1982) 288-289.
3. Postelnicu A, Influence of a magnetic field on heat and mass transfer by natural convection from vertical surfaces in porous media considering Soret and Dufour effects, Int J Heat Mass Trans., 47 (2004) 1467-1472.
4. Cortell R, MHD flow and mass transfer of an electrically conducting fluid of second grade in a porous medium over a stretching sheet with chemically reactive species, Chem. Engg. Processing, 46 (2007) 721-728.
5. Mansour M.A, El-Anssary N.F and Aly A.M, Effects of chemical reaction and thermal stratification on MHD free convective heat and mass transfer over a vertical stretching surface embedded in a porous media considering Soret and Dufour numbers, Chem. Engg. J., 145 (2008) 340–345.
6. Rashidi M.M and Erfani E, A new analytical study of MHD stagnation-point flow in porous media with heat transfer, Comput. & Fluids, 40 (2011) 172–178.

7. Srinivas S, Subramanyam Reddy A and Ramamohan T.R, A study on thermal diffusion and diffusion-thermo effects in a two-dimensional viscous flow between slowly expanding or contracting walls with weak permeability, Int J Heat Mass Transfer, 55 (2012) 3008-3020.
8. Srinivas S, Reddy P.B.A and Prasad B.S.R.V, Effects of chemical reaction and thermal Radiation on MHD flow over an inclined permeable stretching surface with non-uniform heat source/sink: An application to the dynamics of blood flow, J Mech. Med. and Bio., 14 (2014) 1450067-1450091.
9. Muthuraj R, Srinivas S, Shulka A.K and Ramamohan T.R, Effects of thermal-diffusion, diffusion-thermo and space porosity on MHD mixed convective flow of micropolar fluid in a vertical channel with viscous dissipation, Heat Transfer-Asian Res., 43 (2014) 561-576.
10. Lourdu Immaculate D, Muthuraj R, Selvi R.K, Srinivas S and Anant Kant Shukla, The influence of thermophoretic particle deposition on fully developed MHD mixed convective flow in a vertical channel with thermal-diffusion and diffusion-thermo effects, Ain Shams Engg. J., 6 (2015) 671-681.
11. Muthuraj R, Lourdu Immaculate D and Srinivas S, MHD Couette flow of Powell Eyring fluid in an inclined porous space in the presence of temperature dependent heat source with chemical reaction, J Porous Media, 20 (2017) 559-575.
12. Casson N, A flow equation for pigment oil suspensions of the printing ink type.In, Rheology of Disperse Systems, editors. C. C.Mill, London UK: Pergamon Press, (1959) 84–102.
13. Eldabe N.T.M and Salwa M.G.E, Heat transfer of MHD non-Newtonian casson fluid flow between two rotating cylinder, J Physics Soc., Japan, 64 (1995) 41–64.
14. Boyd J, Buick J.M and Green S, Analysis of the Casson and Carreau-Yasuda non-Newtonian blood models in steady and oscillatory flow using the lattice Boltzmann method , Phy. Fluids, 19 (1995) 093103.
15. Nadeem S, Ul Haq R and Lee C, MHD flow of a Casson fluid over an exponentially shrinking sheet, Scientia Iranica, 19 (2012) 1550-1553.
16. Sarojamma G, Vasundhara B and Vendabai K. MHD Casson fluid flow, heat and mass transfer in a vertical channel with stretching walls, Int J Sci. Innovat. Math. Res., 2 (2014) 800-810.
17. Arthur E.M, Seini I.Y and Bortteir L.B, Analysis of Casson fluid flow over a vertical porous surface with chemical reaction in the presence of magnetic field, J Appl. Math. Phy., 3 (2015) 713-723.
18. Khalid A, Khan I, Khan A and Shafie S. Unsteady MHD free convection flow of casson fluid past over an oscillating vertical plate embedded in a porous medium, Engg. Sci. Tech., Int J., 18 (2015) 309-317.
19. Choi S.U.S, Enhancing thermal conductivity of fluids with nanoparticles. In: Siginer DA ,Wang HP, editors, Develop and Applns Non-Newtonian Flows, New York ,ASME, 66 (1995) 99-105.
20. Manimaran B, Thanasekaran P, Rajendran T, Lin R.J, Chang I.J, Lee G.H, Peng S.M, Rajagopal S and Lu K.L, Luminescence enhancement induced by aggregation of alkoxy-Bridged rhenium(I) molecular rectangles, Inorg. Che., 41 (2002)5323-5325.
21. Buongiorno J, Convective transport in nano fluids, ASME J Heat Trans., 128 (2006) 240-250.
22. Kuznetsov A.V and Nield D.A, Natural convective boundary-layer flow of a nanofluid past a vertical plate, Int J Therm. Sci., 49 (2010) 243-247.
23. Noreen S.A and Nadeem S. Endoscopic effects on the peristaltic flow of a nanofluid. Commun. Theoret. Phys., 56 (2011) 761-768.
24. Rana P and Bhargava R, Flow and heat transfer of a nanofluid over a nonlinearly stretching sheet: a numerical study, Commun Nonlinear Sci. and Numer. Simul, 17 (2012) 212-226.
25. Xu H, Fan T and Pop I, Analysis of mixed convection flow of a nanofluid in a vertical channel with the Buongiorno mathematical model, Int Commun Heat Mass Transfer, 44 (2013)15–22.
26. Nadeem S, Mehmood R and Akbar N.S, Optimized analytical solution for oblique flow of a Casson-nano fluid with convective boundary conditions, Int. J Thermal Sci. 78 (2014) 90-100.
27. Khan N.A, Sultan F and Rubbab Q, Optimal solution of nonlinear heat and mass transfer in a two-layer flow with nano Eyring–Powell fluid, Results Phy, 5 (2015) 199– 205.
28. Freidoonimehr N, Rashidi M.M and Mahmud S, Unsteady MHD free convective flow past a permeable stretching vertical surface in a nano-fluid, Int J Thermal Sci, 87 (2015) 136-145.
29. Lourdu Immaculate D, Muthuraj R, Shukla A.K and Srinivas S, MHD unsteady flow of a williamson nanofluid in a vertical porous space with oscillating wall temperature, Front. Heat Mass Transfer, 12 (2016) 14pages.
30. Liao S.J, Beyond Perturbation. Introduction to Homotopy Analysis Method. Boca Raton: Chapman & Hall/CRC Press, 2003.
31. Liao S.J, An optimal homotopy-analysis approach for strongly nonlinear differential equations,

Commun Nonlinear Sci Numer Simul, 15 (2010) 2003 2016
32. Zahedi M.S and Nik H.S, On homotopy analysis method applied to linear optimal control Problems, Appl. Math. Model, 37 (2013) 9617–9629.
33. Hang X and Pop I, Fully developed mixed convection flow in a horizontal channel filled by a nanofluid containing both nanoparticles and gyrotactic microorganisms, Eur. J Mech.- B/Fluids, 46 (2014) 37–45.
34. Shukla A.K, Ramamohan T.R and Srinivas S, A new analytical approach for limit cycles and quasi-periodic solutions for nonlinear oscillators: the example of the forced Van der Pol Duffing oscillator, Phys. Scripta, 89 (2014) 075202.
35. Srinivas S, Shukla A.K, Ramamohan T.R and Reddy A.S, Influence of thermal radiation on unsteady flow over an expanding or contracting cylinder with thermal-diffusion and diffusion-thermo effects, J Aerospace Engg, 28 (2015) 04014134.